

Quasicontinuous Exhaust Scenario for a Fusion Reactor: The Renaissance of Small Edge Localized Modes

G. F. Harrer^{1,2,‡}, M. Faitsch², L. Radovanovic^{1,2}, E. Wolfrum², C. Albert³, A. Cathey², M. Cavedon⁴,
M. Dunne², T. Eich², R. Fischer², M. Griener², M. Hoelzl², B. Labit⁵, H. Meyer⁶, F. Aumayr¹,

The ASDEX Upgrade Team,^{*} and The EUROfusion MST1 Team[†]

¹Institute of Applied Physics, TU Wien, Fusion@ÖAW, Vienna, Austria

²Max Planck Institute for Plasma Physics, Garching, Germany

³Institute of Theoretical and Computational Physics, TU Graz, Graz, Austria

⁴Dipartimento di Fisica "G. Occhialini," Università di Milano-Bicocca, Milano, Italy

⁵École Polytechnique Fédérale de Lausanne (EPFL), Swiss Plasma Center (SPC), CH-1015 Lausanne, Switzerland

⁶CCFE, Culham Science Centre, Abingdon, Oxon, United Kingdom



(Received 28 October 2021; revised 8 July 2022; accepted 8 August 2022; published 10 October 2022)

Tokamak operational regimes with small edge localized modes (ELMs) could be a solution to the problem of large transient heat loads in fusion reactors. A ballooning mode near the last closed flux surface governed by the pressure gradient and the magnetic shear there has been proposed for small ELMs. In this Letter, we experimentally investigate several stabilizing effects near the last closed flux surface and present linear ideal simulations that indeed develop ballooninglike fluctuations there and connect them with nonlinear resistive simulations. The dimensionless parameters of the small ELM regime in the region of interest are very similar to those in a reactor, making this regime the ideal exhaust scenario for a future device.

DOI: 10.1103/PhysRevLett.129.165001

Future devices that exploit nuclear fusion to generate electrical energy must have good particle and energy confinement to achieve enough fusion gain. In tokamaks, an excellent confinement is linked to an edge transport barrier, which is accompanied by steep pressure gradients at the edge, the so-called pedestal [1]. However, the particle confinement must not be too good either, since in steady state operation impurities and the fusion product helium must be removed and replaced by fresh fuel. An additional requirement for large devices is a high density at the last closed flux surface (the separatrix), a condition that must be met to protect the plasma facing components from excessive power loads [2]. The steep pressure gradients at the edge can be the cause of instabilities, so-called edge localized modes (ELMs), which expel both particles and energy in strong bursts. The largest and most common edge localized modes are called type-I ELMs [3]. While still tolerable in present day machines, these type-I ELMs pose a serious threat to first wall components of reactor-grade devices such as the International Thermonuclear Experimental Reactor (ITER) or future DEMONstration

Power Plants [4,5]. The search for mitigation measures (using, e.g., resonant magnetic perturbation coils or pace making of smaller ELMs by pellet injection [6,7]) or even better for operational regimes that avoid such strong bursts while maintaining the good confinement at high separatrix densities has been ongoing for years [8]. The small ELM regime presented in this Letter has been observed on several machines before and was then called the type-II or grassy ELM regime [9–15]. However, at that time the interpretation of the stability of type-II ELMs took place in the same parameter space as for type-I ELMs, namely edge pressure gradient and edge bootstrap current across the whole pedestal width [16]. Type-II ELM scenarios were excluded for a reactor because they occur at pedestal top collisionalities $\nu_e^* \propto n_e/T_e^2$ that are much higher than needed due to the necessary high temperature. In present day machines, collisionalities at the pedestal top and at the separatrix cannot be matched in the same plasmas. In the following we will demonstrate that the small ELMs, in contrast to the disastrous type-I ELMs, are not destabilized in the entire region of the edge transport barrier, but only in a small region just inside the last closed flux surface emphasizing the importance of the matching separatrix collisionality [$\nu_{e,\text{sep}}^*(\text{AUG}_{\text{QCE}}) = \nu_{e,\text{sep}}^*(\text{ITER}) = \mathcal{O}(10)$]. Moreover, by specifically tailoring the pedestal in such a way that the small ELMs provide enough quasicontinuous transport, while reducing the pedestal width, we show that the occurrence of large type-I ELMs can be prevented

Published by the American Physical Society under the terms of the Creative Commons Attribution 4.0 International license. Further distribution of this work must maintain attribution to the author(s) and the published article's title, journal citation, and DOI.

without the need for any mitigation measures. In this way, we can successfully achieve a mode of operation with good confinement at high separatrix density and a wide heat load footprint in the divertor. This tokamak operating regime provides a quasicontinuous exhaust of particles and heat while preventing the occurrence of strong type-I ELMs (therefore termed quasicontinuous exhaust or QCE scenario). It shows enhanced filamentary transport [17] and a significantly broadened heat-flux footprint [18] and is therefore a particularly promising regime for future fusion devices like ITER or future DEMONstration Power Plants.

The realization that this regime benefits from instabilities at the foot of the transport barrier [19,20], which lead to quasicontinuous transport without significantly degrading confinement, has led us to investigate the factors that can tailor the instabilities. These investigations show that, while the driving pressure gradient is mainly determined by density, the dominant destabilizing terms are a weak local magnetic shear, a weak poloidal flow shear, and a long connection length between the bad curvature low field side (LFS) and the good curvature high field side (HFS). We could meanwhile experimentally demonstrate and establish the QCE regime for a wide range of safety factors and heating powers. Moreover, ideal ballooning stability calculations show that, in all discharges, the narrow region just inside the separatrix is ideally ballooning unstable. First, nonlinear, resistive magnetohydrodynamic calculations of such a small ELM regime using the JOREK code [21] develop ballooninglike fluctuations under similar conditions such as an elevated separatrix density. We can therefore state that the new understanding of the origin of the small ELM regime, namely a localized unstable region just inside the separatrix, is supported by several experimental findings as well as linear ideal and nonlinear resistive modeling.

To emphasize the broad operational range of the QCE regime, this Letter focuses on three discharges at safety factors of $q_{95} = 4, 6, \text{ and } 8$, achieved by a variation of plasma current and toroidal field, performed on ASDEX Upgrade close to the empirical density limit $f_{\text{GW,ped}} > 0.87$ and ITER confinement timescaling factors $H_{98,y2} > 1$. The difference of the two methods for the q_{95} scan, namely altering B_T and I_p , were found to be negligible for this study. This has been analyzed with additional discharges that are not shown in this Letter. All three presented discharges were programmed to have a high elongation and triangularity (solid line cross section in Fig. 1, left) resulting in a small ELM dominant phase. To influence the connection length between the good and bad curvature side $l_{\text{HFS} \rightarrow \text{LFS}}$ (measured at a poloidal radius of $\rho_{\text{pol}} = 0.99$ depicted by the red arrow in Fig. 1), and therefore the ballooning stability, the plasma shapes were then altered in the same way (dotted cross section in Fig. 1) for all three discharges. The temporal evolution of $l_{\text{HFS} \rightarrow \text{LFS}}$ as well as q_{95} is depicted on the right of Fig. 1.

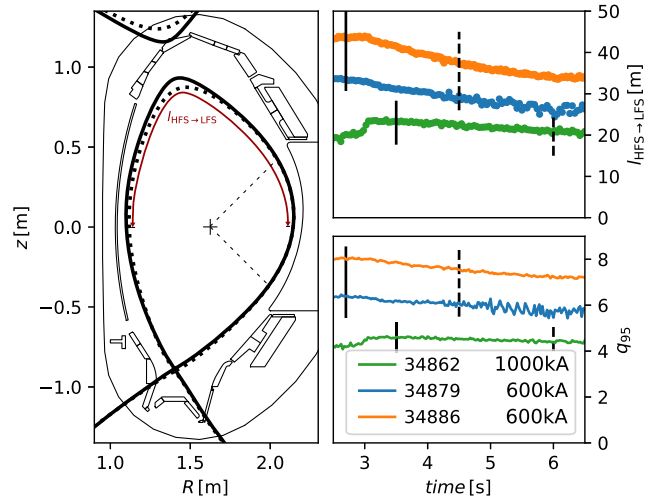


FIG. 1. Left: Cross section of the separatrix of the high (solid) and low (dashed) $l_{\text{HFS} \rightarrow \text{LFS}}$ time points. $l_{\text{HFS} \rightarrow \text{LFS}}$ is the length of a field line spanning from the LFS to the HFS midplane. A poloidal projection of $l_{\text{HFS} \rightarrow \text{LFS}}$ is depicted with the red arrow. Right: Temporal evolution of $l_{\text{HFS} \rightarrow \text{LFS}}$ and the safety factor at 95% flux throughout the three discharges.

The outer poloidal divertor current, measured in the scrape-off layer (SOL), I_{polSOLa} , serving as an ELM indicator in metal machines, is shown in Fig. 2 for all three discharges, including offsets of 20 kA for illustrative purposes. The small ELM regime is established at 3 s in the lowest q discharge (#34862) and at 2 s in the other two discharges. One second later, the plasma z position is gradually ramped down, consequently reducing $l_{\text{HFS} \rightarrow \text{LFS}}$. In all three discharges, at the time of the longest connection between LFS and HFS (black solid bar), the largest transport caused by the small ELMs is observable as an

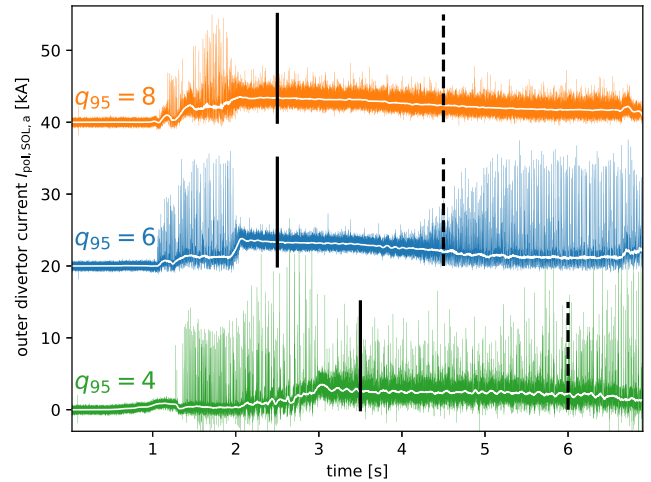


FIG. 2. ELM signatures of the three discharges with different edge safety factors. The two higher q discharges are offset by 20 kA and 40 kA for better visibility. The solid and dashed lines mark the higher and lower connection length configurations depicted in Fig. 1.

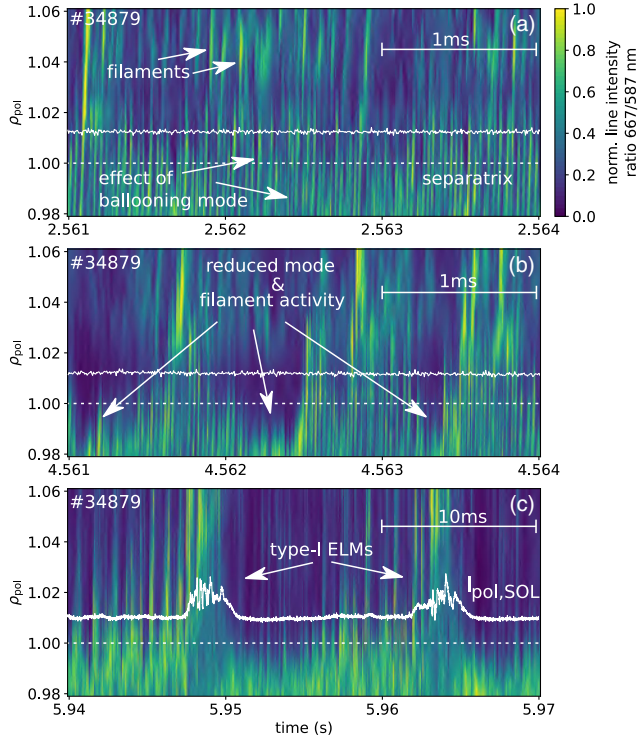


FIG. 3. Pedestal bottom ballooning mode and SOL filaments measured via thermal helium beam spectroscopy. Overlaid in white divertor current as an ELM monitor and the separatrix position (dashed line). The pure small ELM phase (a) shows a coherent ballooning mode inside the separatrix with many filaments traveling through the SOL. In (b) the ballooning mode activity inside the separatrix is occasionally reduced, which directly lowers the filament activity. (c) shows a longer 30 ms time window depicting two large type-I ELMs.

elevated background in the signals (white lines). With the reduction of the connection length, this background decreases in all three cases, whereby in the high- q discharge no type-I ELMs appear, in the medium- q discharge at 4.5 s the first type-I ELMs arise, and in the low- q discharge type-I ELMs occur sporadically during the entire phase, indicating that the pedestal in the low- q discharge is still very close to the peeling-ballooning stability boundary.

Experimentally, the effect of the ballooning mode inside the separatrix, small ELM filaments as well as large type-I ELM crashes, can be directly observed using thermal helium spectroscopy [22]. Figure 3 depicts the normalized emission intensity ratio of two neutral helium lines, which is proportional to electron temperature and density. Figures 3(a) and 3(b) show 3 ms long time windows of the $q = 6$ discharge as a function of ρ_{pol} . The separatrix position is denoted with a white dashed line, dividing the SOL on the top from the confined region at the bottom. In the confined and near SOL region, the impact of the ballooning mode is visible as a coherent structure with a frequency of around 30 kHz. Neither the exact location nor the structure of the mode can be experimentally determined

using radially resolved 1D He spectroscopy. This mode causes filaments to propagate radially outward and reach the far SOL with a mean occurrence rate of 1 kHz. Whereas the mode and thus the filamentary transport is continuously present in Fig. 3(a), the mode appearance is occasionally weakened at time point 2 s later [Fig. 3(b)]. Here, at lower $l_{\text{HFS} \rightarrow \text{LFS}}$, the plasma is in a mixed ELM regime where the ballooning mode inside the separatrix is less coherent at around 40 kHz and the filament occurrence rate is reduced to 250 Hz. This points to the transport being less continuous with the reduced connection length. This reduction of continuous transport manifests in the appearance of ELMs with increasing amplitude, as seen in the blue time trace of Fig. 2. Figure 3(c) shows a 30 ms time window of this later stage of the discharge, where clear type-I ELMs are present. The time window is 10 times longer compared to Figs. 3(a) and 3(b) to cover the whole ELM evolution. The impact of these large ELMs is seen in the divertor current measurement (white time trace in Fig. 3) and the massively increased radial transport by ELM filaments in the SOL, which clearly dominate the inter-ELM filaments that are still present.

In addition to the influence of the high-field side, there are also local mechanisms governing the small ELM stability, especially the local magnetic shear $s_l = -e_{\perp} \cdot \nabla \times e_{\perp}$ as defined in [23] with $e_{\perp} = (\nabla \Psi / \|\nabla \Psi\|) \times (B / \|B\|)$. s_l represents the local tilt of neighboring flux tubes and can stabilize ballooning modes, in particular the ones at the pedestal bottom causing the small ELMs at the LFS.

Figure 4 shows a measure of the shear stabilization of the bad curvature region around the LFS midplane achieved by integrating the local magnetic shear poloidally along the field lines from -45° to 45° with regard to the midplane at

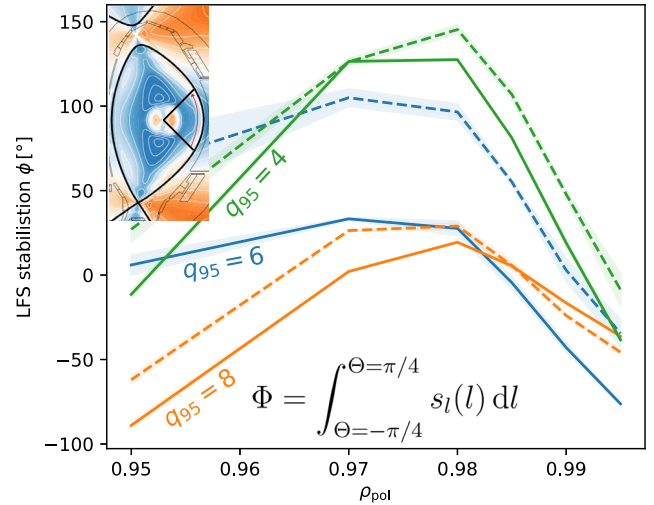


FIG. 4. Shear stabilization at the bad curvature side represented by the field line integrated local magnetic shear from -45° to 45° with regard to the outboard midplane. Solid lines show the high and dashed lines the lower $l_{\text{HFS} \rightarrow \text{LFS}}$ phases. Different colors represent the different safety factors.

different radial positions. Here, the solid lines represent the high connection length phases while the connection length phases are depicted with dashed lines. In the high- q case, which stays in the small ELM regime, lowering the connection length only changes the stabilization inside $\rho = 0.98$. The medium- and high- q cases show an increase of the shear stabilization at the separatrix, which is in agreement with the observed transport behavior, i.e., a stabilization of the small ELMs located at the pedestal foot.

The ballooning stability of the three discharges was calculated with HELENA [24] using high resolution IDE [25] equilibria to guarantee an accurate bootstrap current evolution. HELENA, an ideal $n \rightarrow \infty$ code, calculates the linear stability at each flux surface separately, which results in profiles for the critical normalized pressure gradient α_{crit} at which the plasma would become ballooning unstable. Although the resistivity is quite high in the region of interest, ideal analysis provides a good first step as it has recently been shown that including resistivity only lowers the stability boundary [26,27]. The experimental normalized pressure gradient, i.e., the ballooning drive close to the separatrix, stays constant within measurement tolerances with the change of the connection length for all three discharges. The temporal evolution of the marginal stability $F_{\text{marg}} = \alpha_{\text{crit}}/\alpha_{\text{exp}}$ of the three discharges is plotted for different radial positions and shows some distinct features that can be summarized as follows: When the discharge evolves to the high shaping (3 s for 34862, 2 s for the higher q discharges), the plasma becomes ideal ballooning unstable close to the separatrix at $\rho = 0.99$. In the steep gradient region at $\rho = 0.98$, the plasmas are more stable (scans in s - α space show second stability access). After the connection length is lowered, the outer unstable region gets shifted even further outward and the region of stability becomes broader. The effect is best seen in the medium- q shot [Fig. 5(b)], where it leads to a broadening of the pedestal and a reappearance of type-I ELMs resulting in a mixed ELM regime. The location of the small ELMs lies further inside the plasma in the pure small ELM phases. In the mixed regime, it is shifted outside into a region of lower pressure, which is why the small ELMs cause less transport there and type-I ELMs are again present. The lower LFS shear stabilization as well as the higher $l_{\text{HFS} \rightarrow \text{LFS}}$ in the high- q case keep the plasma in the small ELM regime. QCE or small ELM filaments are observed in all discharges when the ballooning instability at the pedestal bottom is present.

The third quantity crucial for edge stability is the radial electric field and the associated flow shear, the $E \times B$ shear, or in other words the radial change of the $E \times B$ velocity. Its main ingredient is the gradient of the radial electric field, which is notoriously hard to measure experimentally. It has been reported to suppress turbulent transport and is widely believed to be the main cause for the L-H transition [28–30]. To investigate its role in small ELM stability, the radial electric field E_r profiles for the two higher q

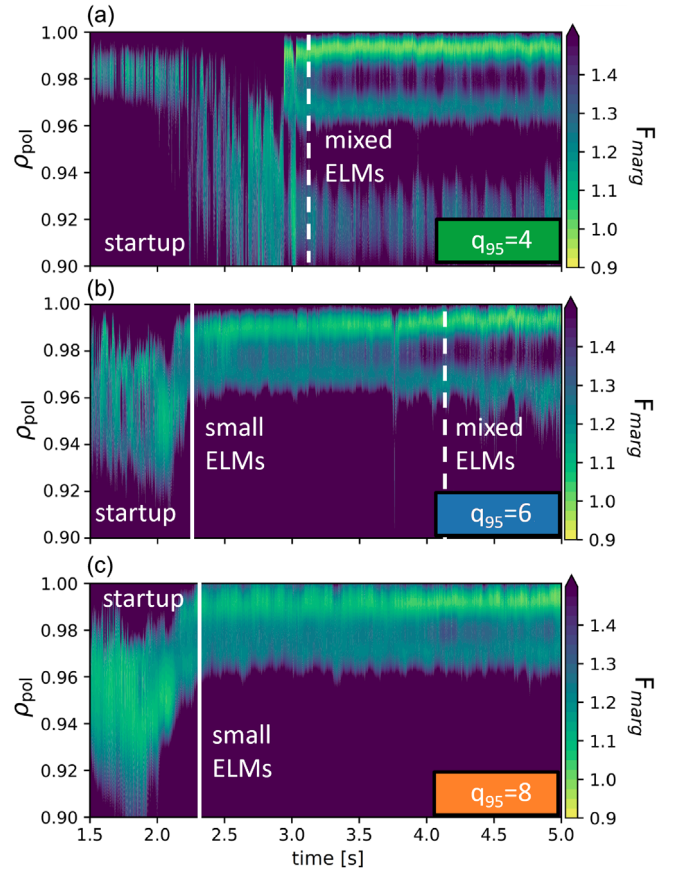


FIG. 5. Time traces of the marginal stability F_{marg} of three QCE discharges [(a) $q_{95} = 4$, (b) $q_{95} = 6$, and (c) $q_{95} = 8$] for different ρ_{pol} . The transitions of dominant ELM type are marked with white vertical lines. Ballooning stability is represented by dark blue colors while instability is colored in light green.

discharges have been calculated from the line intensity and the poloidal and toroidal velocity measured by the AUG charge exchange recombination spectroscopy diagnostics using the radial force balance. The profile reconstruction for the lowest q discharge showed a minimum of E_r outside the separatrix, suggesting that the measurements were affected by the type-I ELMs. The discharge has therefore been left out of this analysis.

The data points measured are shown in Fig. 6 as circles for the higher $l_{\text{HFS} \rightarrow \text{LFS}}$ and crosses for the lowered $l_{\text{HFS} \rightarrow \text{LFS}}$ phases. The E_r data were then fitted using the proFit Gaussian process routine [31] with a squared exponential kernel. The right side of Fig. 6 shows the fitted profiles for the two discharges, where again solid lines denote the higher and dashed lines the $l_{\text{HFS} \rightarrow \text{LFS}}$ phases. While radial electric field profiles in the $q_{95} = 8$ case (orange) do not change with the alteration of the plasma shape, the characteristic minimum in the E_r profile becomes 50% deeper in the $q_{95} = 6$ case. This could be due to the influence of the already occurring type-I ELMs in the mixed ELM phase.

The HELENA ballooning stability calculations presented in Fig. 5 do not take the $E \times B$ shear into account. As the E_r

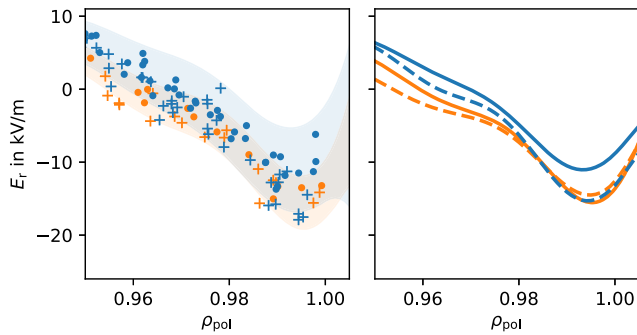


FIG. 6. Radial electric field measured with charge exchange recombination spectroscopy of the $q_{95} = 6$ (blue) and $q_{95} = 8$ (orange) discharges, including a Gaussian process fit of the data on the right-hand side. Dots and full lines represent the high $l_{\text{HFS} \rightarrow \text{LFS}}$ phases, while crosses and dashed lines depict lower $l_{\text{HFS} \rightarrow \text{LFS}}$.

profiles and also their gradients change significantly when comparing the clean small ELM phase with the phase where type-I ELMs reappear, the influence of the $E \times B$ shear on small ELM stability cannot be disregarded.

Recently, full type-I ELM cycles have been simulated with the nonlinear resistive magnetohydrodynamic JOREK code [32]. By using similar plasma parameters, we were able to show simulations with small ELMs with less impact on the divertor. The simulations exhibit growth of a broad spectrum of mode numbers without a clearly dominating one and an enhanced pressure gradient close to the separatrix. With increased heating power and/or by decreasing the separatrix density, the E_r well deepens, leading to a reoccurrence of type-I ELMs in the simulation. A detailed description of the simulation results can be found in [33].

The simulations point to the important role of the $E \times B$ shear, as without it, JOREK is not able to reproduce ELM cycles of a small or large kind and can only simulate single ELM events followed by unrealistically strong ballooning turbulence [34].

All three stabilizing quantities—magnetic shear, $E \times B$ shear, and the connection length between good and bad curvature regions—can and do change with the shape changes and influence the amount of transport induced by the small ELMs. The consequently changed shape of the whole pedestal appears to be the crucial factor determining the occurrence of large ELMs. It has to be stated here that the lowest q case presented exhibits type-I ELMs throughout the discharge, which would be disastrous for a reactor. With a higher plasma triangularity and thus an increased $l_{\text{HFS} \rightarrow \text{LFS}}$ and lower separatrix shear stabilization, pure QCE discharges without any type-I ELMs have already been performed at AUG up to values of $q_{95} = 3.6$ (using $I_p = 1$ MA and $B_T = 2$ T). The similarity of the normalized pedestal bottom conditions in the QCE discharges to the ones that are predicted in larger devices, especially the separatrix collisionality, have already motivated stability analyses of ITER equilibria that also show ballooning instability of the pedestal bottom [35]. Although the

pressure gradient at the separatrix is hard to predict, with the separatrix densities expected to be fairly similar, the temperatures are, however, higher at the separatrix but especially at the pedestal top. The connection length to the stabilizing HFS is larger and could therefore play a bigger role; the flow shear, on the other hand, is proportional to $1/B$ and is therefore lower. Only a code that can take into account all these different mechanisms simultaneously will be able to make reasonable predictions.

To summarize, we have revisited a promising operational regime for magnetically confined fusion devices, analyzed the conditions under which the devices must be operated to achieve this regime, and performed (linear and non-linear) modeling calculations to support our interpretation. The new understanding of the QCE scenario makes us confident that such a regime is the best option for future reactor-grade machines.

G. F. H., a former fellow of the Friedrich Schiedel foundation for energy technology, is the recipient of a EUROfusion researcher grant. This work has been carried out within the framework of the EUROfusion consortium and has received funding from the Euratom research and training programme 2014-2018 and 2019-2020 under grant agreement no. 633053. The views and opinions expressed herein do not necessarily reflect those of the European Commission.

*See author list of H. Meyer *et al.*, Overview of physics studies on ASDEX Upgrade, Nucl. Fusion 59, 112014 (2019).

†See author list of B. Labit *et al.*, Dependence on plasma shape and plasma fueling for small edge-localized regimes in TCV and ASDEX Upgrade, Nucl. Fusion 59, 086020 (2019).

‡Corresponding author.
harrer@iap.tuwien.ac.at

- [1] F. Wagner, G. Becker, K. Behringer, D. Campbell *et al.*, Regime of Improved Confinement and High Beta in Neutral-Beam-Heated Divertor Discharges of the ASDEX Tokamak, *Phys. Rev. Lett.* **49**, 1408 (1982).
- [2] M. Wischmeier, High density operation for reactor-relevant power exhaust, *J. Nucl. Mater.* **463**, 22 (2015).
- [3] H. Zohm, Edge localized modes (ELMs), *Plasma Phys. Controlled Fusion* **38**, 105 (1996).
- [4] B. Riccardi, R. Giniatulin, N. Klimov, V. Koidan, and A. Loarte, Preliminary results of the experimental study of PFCS exposure to ELMs-like transient loads followed by high heat flux thermal fatigue, *Fusion Eng. Des.* **86**, 1665 (2011).
- [5] T. Eich, B. Sieglin, A. J. Thornton, M. Faitsch, A. Kirk, A. Herrmann, and W. Suttrop, ELM divertor peak energy fluence scaling to ITER with data from JET, MAST and ASDEX upgrade, *Nucl. Mater. Energy* **12**, 84 (2017).
- [6] R. Nazikian, C. Paz-Soldan, J. D. Callen, J. DeGrassie *et al.*, Pedestal Bifurcation and Resonant Field Penetration at the Threshold of Edge-Localized Mode Suppression in the DIII-D Tokamak, *Phys. Rev. Lett.* **114**, 105002 (2015).

- [7] L. R. Baylor, N. Commaux, T. C. Jernigan, N. H. Brooks *et al.*, Reduction of Edge-Localized Mode Intensity Using High-Repetition-Rate Pellet Injection in Tokamak H-Mode Plasmas, *Phys. Rev. Lett.* **110**, 245001 (2013).
- [8] E. Viezzer, Access and sustainment of naturally ELM-free and small-ELM regimes, *Nucl. Fusion* **58**, 115002 (2018).
- [9] T. Ozeki and M. Azumi, Access to the second stability regime near the plasma surface in a high- q , low-shear Tokamak plasma, *J. Phys. Soc. Jpn.* **59**, 927 (1990).
- [10] G. Saibene, P. Lomas, R. Sartori, A. Loarte *et al.*, Characterization of small ELM experiments in highly shaped single null and quasi-double-null plasmas in JET, *Nucl. Fusion* **45**, 297 (2005).
- [11] J. Stober, P. Lomas, G. Saibene, Y. Andrew *et al.*, Small ELM regimes with good confinement on JET and comparison to those on ASDEX Upgrade, Alcator C-mod and JT-60U, *Nucl. Fusion* **45**, 1213 (2005).
- [12] A. Kirk, H. Muller, E. Wolfrum, H. Meyer, A. Herrmann, T. Lunt, V. Rohde, and P. Tamain, Comparison of small edge-localized modes on MAST and ASDEX Upgrade, *Plasma Phys. Controlled Fusion* **53**, 095008 (2011).
- [13] N. Oyama, P. Gohil, L. Horton, A. Hubbard, J. Hughes, Y. Kamada, K. Kamiya, A. Leonard, A. Loarte, R. Maingi, G. Saibene, R. Sartori, J. Stober, W. Suttrop, H. Urano, W. West, and t. I. P. T. Group, Pedestal conditions for small ELM regimes in Tokamaks, *Plasma Phys. Controlled Fusion* **48**, A171 (2006).
- [14] E. Wolfrum, M. Bernert, J. Boom, A. Burckhart *et al.*, Characterization of edge profiles and fluctuations in discharges with type-II and nitrogen-mitigated edge localized modes in ASDEX Upgrade, *Plasma Phys. Controlled Fusion* **53**, 085026 (2011).
- [15] G. S. Xu, Q. Q. Yang, N. Yan, Y. F. Wang, X. Q. Xu, H. Y. Guo, R. Maingi, L. Wang, J. P. Qian, X. Z. Gong, V. S. Chan, T. Zhang, Q. Zang, Y. Y. Li, L. Zhang, G. H. Hu, and B. N. Wan, Promising High-Confinement Regime for Steady-State Fusion, *Phys. Rev. Lett.* **122**, 255001 (2019).
- [16] P. Snyder, H. Wilson, J. Ferron, L. Lao, A. Leonard, D. Mossessian, M. Murakami, T. Osborne, A. Turnbull, and X. Xu, ELMs and constraints on the H-mode pedestal: Peeling-ballooning stability calculation and comparison with experiment, *Nucl. Fusion* **44**, 320 (2004).
- [17] M. Griener, E. Wolfrum, G. Birkenmeier, M. Faitsch, R. Fischer, G. Fuchert, L. Gil, G. F. Harrer, P. Manz, D. Wendler, and U. Stroth, Continuous observation of filaments from the confined region to the far scrape-off layer, *Nucl. Mater. Energy* **25**, 100854 (2020).
- [18] M. Faitsch, T. Eich, G. F. Harrer, E. Wolfrum, D. Brida, P. David, M. Griener, and U. Stroth, Broadening of the power fall-off length in a high density, high confinement H-mode regime in ASDEX Upgrade, *Nucl. Mater. Energy* **26**, 100890 (2021).
- [19] G. F. Harrer, E. Wolfrum, M. Dunne, P. Manz, M. Cavedon, P. Lang, B. Kurzan, T. Eich, B. Labit, J. Stober, H. Meyer, M. Bernert, F. Lagner, and F. Aumayr, Parameter dependences of small edge localized modes (ELMs), *Nucl. Fusion* **58**, 112001 (2018).
- [20] B. Labit, T. Eich, G. Harrer, E. Wolfrum *et al.*, Dependence on plasma shape and plasma fuelling for small edge-localized mode regimes in TCV and ASDEX Upgrade, *Nucl. Fusion* **59**, 086020 (2019).
- [21] M. Hoelzl, G. Huijsmans, S. Pamela, M. Bécoulet *et al.*, The JOREK non-linear extended MHD code and applications to large-scale instabilities and their control in magnetically confined fusion plasmas, *Nucl. Fusion* **61**, 065001 (2021).
- [22] M. Griener, O. Schmitz, K. Bald, D. Bösser, M. Cavedon, P. De Marné, T. Eich, G. Fuchert, A. Herrmann, A. Kappatou, T. Lunt, V. Rohde, B. Schweer, M. Sochor, U. Stroth, A. Terra, and E. Wolfrum, Fast piezoelectric valve offering controlled gas injection in magnetically confined fusion plasmas for diagnostic and fuelling purposes, *Rev. Sci. Instrum.* **88**, 033509 (2017).
- [23] P. J. Mc Carthy, Practical expressions for local magnetic shear, normal and geodesic curvatures in an axisymmetric plasma equilibrium of arbitrary cross-section, *Plasma Phys. Controlled Fusion* **55**, 085011 (2013).
- [24] G. Huysmans, J. Goedbloed, and W. Kerner, Isoparametric bicubic Hermite elements for solution of the Grad-Shafranov equation, *Int. J. Mod. Phys. C* **02**, 371 (1991).
- [25] R. Fischer, A. Bock, M. Dunne, J. Fuchs, L. Giannone, K. Lackner, P. McCarthy, E. Poli, R. Preuss, M. Rampp, M. Schubert, J. Stober, W. Suttrop, G. Tardini, and M. Weiland, Coupling of the flux diffusion equation with the equilibrium reconstruction at ASDEX upgrade, *Fusion Sci. Technol.* **69**, 526 (2016).
- [26] N. Wu, S. Chen, M. Mou, C. Tang, X. Song, Z. Yang, D. Yu, J. Xu, M. Jiang, X. Ji, S. Wang, B. Li, and L. Liu, Study on edge localized mode during plasma vertical swing in HL-2A Tokamak, *Phys. Plasmas* **25**, 102505 (2018).
- [27] A. Kleiner, N. Ferraro, A. Diallo, and G. Canal, Importance of resistivity on edge-localized mode onset in spherical Tokamaks, *Nucl. Fusion* **61**, 064002 (2021).
- [28] K. Burrell, T. Carlstrom, E. Doyle, D. Finkenthal *et al.*, Physics of the L-mode to H-mode transition in Tokamaks, *Plasma Phys. Control. Fusion* **34**, 1859 (1992).
- [29] F. Wagner, A quarter-century of H-mode studies, *Plasma Phys. Controlled Fusion* **49**, B1 (2007).
- [30] M. Cavedon, G. Birkenmeier, T. Pütterich, F. Ryter, E. Viezzer, E. Wolfrum, R. Dux, T. Happel, P. Hennequin, U. Plank, U. Stroth, and M. Willensdorfer, Connecting the global H-mode power threshold to the local radial electric field at ASDEX Upgrade, *Nucl. Fusion* **60**, 066026 (2020).
- [31] C. Albert, M. Kendler, R. Babin, M. Hadwiger, R. Hofmeister, M. Khallaayoune, F. Kramp, K. Rath, and B. Rubino-Moyner, proFit: Probabilistic response model fitting with interactive tools (2022), [10.5281/zenodo.6624446](https://doi.org/10.5281/zenodo.6624446).
- [32] A. Cathey, M. Hoelzl, K. Lackner, G. Huijsmans, M. Dunne, E. Wolfrum, S. Pamela, F. Orain, and S. Günter, Non-linear extended MHD simulations of type-I edge localised mode cycles in ASDEX Upgrade and their underlying triggering mechanism, *Nucl. Fusion* **60**, 124007 (2020).
- [33] A. Cathey, M. Hoelzl, G. Harrer, M. G. Dunne, G. T. A. Huijsmans, K. Lackner, S. J. P. Pamela, E. Wolfrum, and S. Günter, MHD simulations of small ELMs at low triangularity in ASDEX Upgrade, *Plasma Phys. Controlled Fusion* **64**, 054011 (2022).

- [34] F. Orain, M. Bécoulet, G. T. A. Huijsmans, G. Dif-Pradalier, M. Hoelzl, J. Morales, X. Garbet, E. Nardon, S. Pamela, C. Passeron, G. Latu, A. Fil, and P. Cahyna, Resistive Reduced MHD Modeling of Multi-Edge-Localized-Mode Cycles in Tokamak X-Point Plasmas, *Phys. Rev. Lett.* **114**, 035001 (2015).
- [35] L. Radovanovic, M. Dunne, E. Wolfrum, G. Harrer, M. Faitsch, R. Fischer, and F. Aumayr, Developing a physics understanding of the quasi-continuous exhaust regime: pedestal profile and ballooning stability analysis, *Nucl. Fusion* **62**, 086004 (2022).